Invited Paper

Monolithic Wavelength-Selective Switches and Cross Connects with Integrated MEMS Mirror Array

Chao-Hsi Chi and Ming C. Wu
Department of Electrical Engineering and Computer Sciences
University of California, Berkeley, CA, USA 94720-1770

ABSTRACT

Wavelength-selective switches (WSSs) and wavelength-selective cross connects (WSXCs) enable flexible, intelligent wavelength-division-multiplexed (WDM) networks as well as reduce the operating cost. In a 1xN WSS, the wavelengths from the input port can be independently switched to any of the N output ports. WSXC allows switching of optical signals at wavelength level between N input ports and N output ports. Most of the WSS and WSXC reported to date are realized by free-space optical systems with either micro-electro-mechanical-systems (MEMS) or liquid crystal (LC) beamsteering array, or by silica-based planar lightwave circuits with cascaded 2x2 thermal optical switches. In this paper, we report on the approach to monolithically integrate the WSS and WSXC on a single silicon-on-insulator (SOI) chip. Optical waveguides, microgratings, parabolic reflectors, as well as MEMS active switching micromirrors are fabricated on the same substrate using a one-step etching process. We have successfully fabricated a 1x4 WSS with CWDM (20-nm) channel spacing on a 1x2-cm^2 chip, and achieved a fiber-to-fiber insertion loss of 11.7 dB, and a switching time of 0.5 msec. The monolithic 4x4 WSXC is realized by integrating four 4x1 WSSs and four 1x4 multi-mode interference (MMI) splitters on the same wafer. No fiber connections or external splitter are required. The fabricated 4x4 WSXC has a chip area of 3.2x4.6 cm^2 and an insertion loss of 24 dB, including a 6-dB splitting loss. The WSXC supports unicast, multicast, and broadcast functions. The devices can be further scaled to DWDM (100-GHz) channel spacing.

Keywords: MEMS, grating, micromirror, optical switch, optical crossconnect, OXC, wavelength-selective switch, WSS, wavelength-selective cross connect, WSXC.

1. INTRODUCTION

With the rapid growth of both internet traffic and diversity of services, technologies have been developed to provide not only larger bandwidth, but also flexible and reconfigurable networks. Time-division multiplexing (TDM) and wavelength-division multiplexing (WDM) are two complementary approaches to increase the transmission capacity by increasing the bit rate and the number of wavelength channels, respectively. Furthermore, the WDM approach enables circuit-switched optical paths for applications such as rapid provisioning and bandwidth on demand. These applications require wavelength-level management of the network.

Wavelength-selective switches (WSSs) and wavelength-selective cross connects (WSXCs) allows switching of optical signals at wavelength level between multiple ports. Demultiplexers and active switches are key elements of WSS and WSXC design. Most of the WSSs and WSXCs reported to date use diffraction gratings or arrayed-waveguide gratings (AWGs) as demultiplexers. The 1xN or NxN active switching can be realized by cascaded 2x2 thermo-optical (TO) switches [1, 2] or MEMS piston-mirror switches [3], or beamsteering array of micro-electro-mechanical-systems (MEMS) [4-10] or liquid crystal (LC) [11]. The approach of cascaded 2x2 switches have advantages of compactness and predefined optical path, but the scaling to higher port counts involves a large amount of switches and high operation cost. On the other hand, the beamsteering mechanism is advantageous for scaling of port counts; however, the reported free-space system [4-8] and hybrid MEMS-waveguide systems [9, 10] require large space and complicated optical alignment. In this paper, we report on the approach to monolithically integrate WSS and WSXC on a single silicon-on-insulator (SOI) chip [12, 13]. Optical waveguides, microgratings, collimating reflectors, focusing reflectors, and MEMS active switching micromirrors are fabricated on the same substrate using a one-step etching process.

Optomechatronic Micro/Nano Devices and Components II, edited by Yoshitada Katagiri,
Proc. of SPIE Vol. 6376, 63760G, (2006) · 0277-786X/06/$15 · doi: 10.1117/12.687121

2. OPTICAL SYSTEM DESIGN

2.1 1xN wavelength-selective switches

The schematic of the monolithic 1x4 WSS is shown in Fig.1. The device consists of five 5μm-wide waveguides. Port 1 is used as the input, and port 2 to 5 as the output. To minimize the spherical and chromatic aberration, parabolic reflectors are used for collimation and focusing. The input WDM signals are collimated by the collimating reflector, and demultiplexed by the micrograting. The micromirror array is integrated at the focal plane of the focusing reflector for independent switching of the wavelength channels. The reflected light propagates in the reverse direction, where it is collimated by the focusing reflector, re-multiplexed by the micrograting, focused by the collimating reflector, and finally coupled to the desired output waveguides.

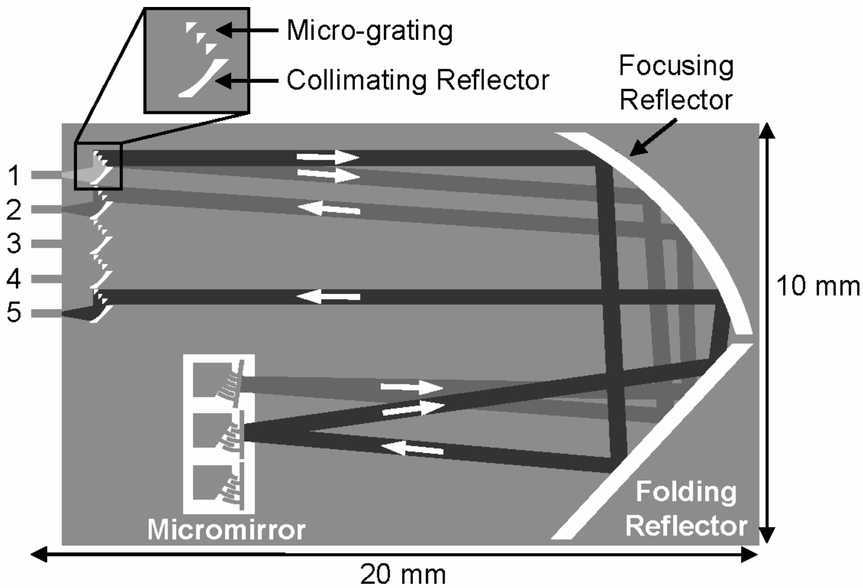

Fig. 1. Schematic of the monolithic 1x4 MEMS wavelength-selective switch. Optical waveguides, microgratings, parabolic reflectors, folding reflectors, and MEMS micromirrors are fabricated on the same SOI substrate.

The micrograting consists of an array of deep etched triangular elements blazed for the 14^{th} order diffraction at 90° angle. The period is 4.5 μm, allowing the WSS to be patterned by i-line optical lithography. The corresponding dispersion strength is 0.074°/nm. Using a 45°-folding reflector, the device footprint is reduced to 1x2 cm^2. The 8-element micromirror array matching to the CWDM (1470-1610 nm) grids (20-nm spacing) is integrated at the focal plane of the focusing reflector. It has a pitch of 400 μm and the corresponding focal length of the focusing reflector is 15.5 mm. The required mechanical scan angle is 1.6° for switching between adjacent ports with 250-μm spacing. A mechanical scan angle of 4.8° is required for the 1x4 WSS. Each MEMS mirror is actuated by a rotary comb-drive actuator. All components are monolithically fabricated on the same silicon-on-insulator (SOI) substrate with a 5-μm-thick device layer. The SOI platform is particularly attractive because it is compatible with SOI PLC as well as SOI-MEMS technologies. All optical paths are defined by photolithography and no optical alignment is necessary. Microgratings, parabolic reflectors, and folding reflectors utilize total internal reflection (TIL). All silicon-air interfaces are anti-reflection (AR)-coated with 180-nm-thick low-stress silicon nitride (n = 2.15). The micromirror is coated with aluminum to enhance its reflectivity. The 4-*f* configuration is used to ensure the geometric focusing position occurs at the minimum spot size of the Gaussian beam. Moreover, the focused spot size on the MEMS micromirror can be adjusted by changing the focal length of collimators independently.

2.2 NxN wavelength-selective cross connects

A 4x4 WSXC can be realized by using 1x4 WSSs as building elements with architectures shown in Fig. 2. It can be made by cascading either four 1x4 WSSs with four 4x1 WSSs (Fig. 2(a)), or four passive 1x4 splitters with four 4x1 WSSs (Fig. 2(b)). The latter has a fundamental splitting loss of 6 dB but it allows broadcast and multicast functions; its smaller chip area (~ 60% of the 8-WSS approach) also makes it very attractive for monolithic integration.

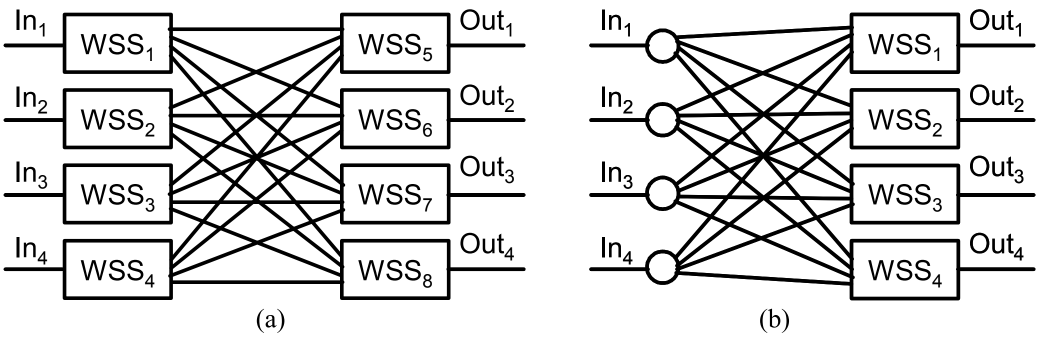

Fig. 2. Architectures of 4x4 WSXC built with (a) four 1x4 WSSs and four 4x1 WSSs (b) four 1x4 passive splitters and four 4x1 WSSs.

The schematic of the monolithic 4x4 WSXC is shown in Fig. 3. Four 4x1 WSSs and four 1x4 splitters are interconnected on the same SOI wafer. No fiber connections or external splitter are required. The input signals are broadcasted to each WSS by the 1x4 multimode interference (MMI) splitter. In each WSS, port 1 is used as output and port 2 to 5 as inputs. By scanning the micromirror, the signal will be selected from one of the input and switched to the output. The 1x4 splitters and the 4x1 WSSs are connected by waveguides with 90° waveguide bend and 90° waveguide crossing, which minimize insertion loss and crosstalk. The two lower WSSs are flipped vertically to reduce the number of waveguide crossings such that there are no more than 10 crossing in any configuration.

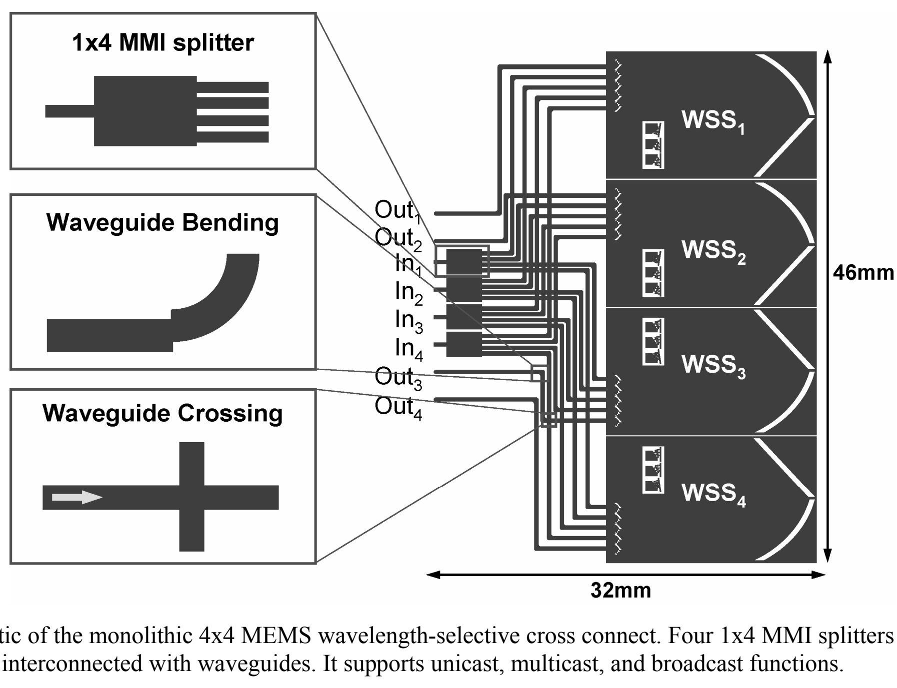

Fig. 3. Schematic of the monolithic 4x4 MEMS wavelength-selective cross connect. Four 1x4 MMI splitters and four 4x1 WSSs are interconnected with waveguides. It supports unicast, multicast, and broadcast functions.

2.3 Scaling of channel spacing

Scaling of channel spacing ($\Delta\lambda$) from coarse WDM (CWDM) grids (20-nm) to dense WDM (DWDM) grids (0.8-nm) needs 25 times higher spectral resolution. This can be accomplished by a longer propagation distance (L) after micrograting, a smaller pitch (P_M) of micromirror array, or a larger angular dispersion (D_λ), as shown by the following relation:

$$\frac{P_M}{L} \approx D_\lambda \cdot \Delta\lambda \tag{1}$$

The propagation distance (L) is limited by the wafer size. For a DWDM 4x4 WSXC to fit in a 6-inch wafer, a micromirror array with a pitch of 75 µm is thus required. The schematic of the micromirror is shown in Fig. 4 [14]. It is actuated by a linear comb-drive. The micromirror is attached through an L-shaped arm to the middle of the flexure spring, which has the largest angular deflection as the comb moves laterally (Fig. 4(b)). The mirror angle is proportional to the displacement, and inversely proportional to the spring length. Short spring length is desired to achieve large mirror angle since the displacement is usually limited by the small pitch. To reduce the operating voltage, we employed a serpentine design, as shown in Fig. 4(c).

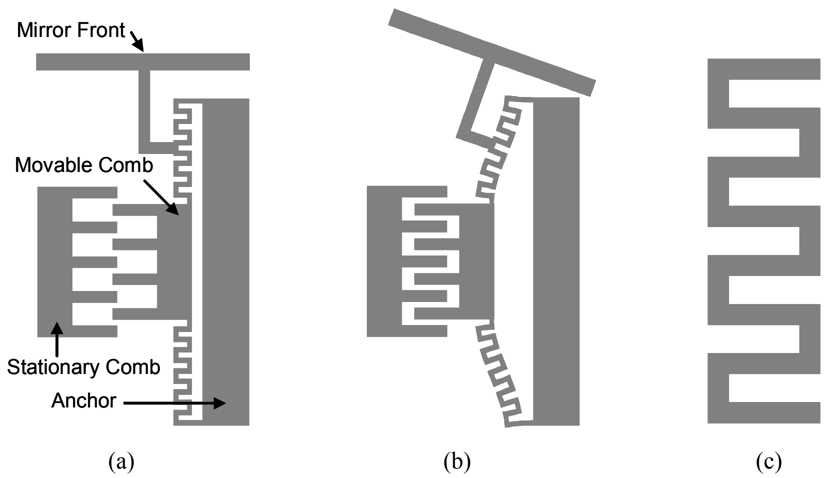

Fig. 4. Schematic of the 75-µm-pitched micromirror with lateral comb-drive actuator (a) without bias, and (b) with non-zero bias. (c) The serpentine spring design.

2.4 Solid immersion micromirror for enhancement of scan angle

Fig. 5(a) shows the schematic of a Si PLC MEMS with a conventional flat micromirror driven by a rotary comb-drive actuator. The angular deflection is reduced by refraction at silicon-air interface, as shown by Snell's law:

$$\theta_{Si} = \sin^{-1}\left(\frac{n_{air}}{n_{Si}} \cdot \sin(\theta_{air})\right) \approx \frac{n_{air}}{n_{Si}} \cdot \theta_{air} \tag{2}$$

where θ_{air} and θ_{Si} are the optical scan angles in the air and silicon, respectively. $n_{air} = 1$ and $n_{Si} = 3.5$ are the refractive indices of air and silicon, respectively. Moreover, the optical beam diverges when propagating in the air gap. It in turn causes a diffraction loss when coupled back to the silicon slab.

We have developed a novel on-chip solid immersion micromirror (SIM) [15], as shown schematically in Fig. 5(b). Instead of using the front Si-air interface, the micromirror is now coated on the back interface. The air gap between the Si slab and the SIM follow a curved contour so that light always passes through the Si-air interface at nearly normal incidence. The deflection angle inside Si slab is enhanced by approximately ~3.5 times compared with conventional flat micromirrors. Since the air gap follows the curved trace of mirror rotation, the gap distance remains constant during rotation. This greatly reduces the diffraction loss, especially for large rotation angle.

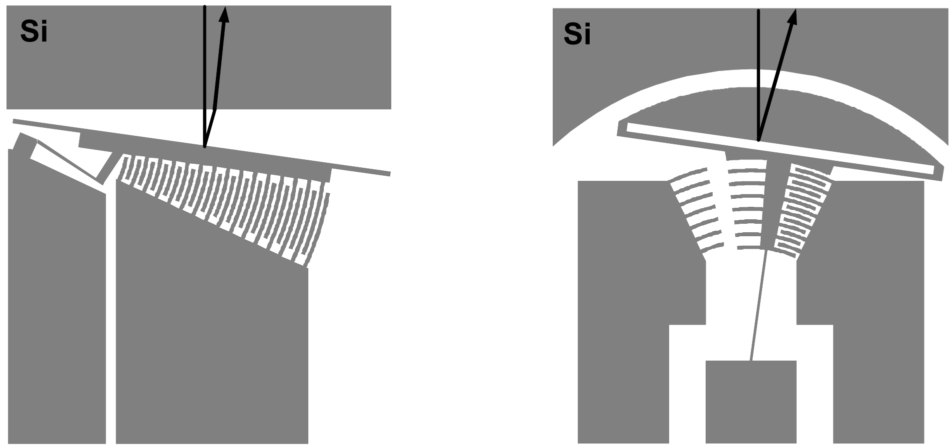

(a) (b)

Fig. 5. Schematic of on-chip micromirrors (a) flat micromirror (b) solid immersion micromirror. The solid immersion micromirror has ~3.5 times enhancement of scan angle.

3. FABRICATION

The CWDM devices were fabricated on a 4-inch silicon-on-insulator (SOI) wafer with a device layer of 5-μm thickness, and a buried silicon dioxide (SiO_2) layer of 2-μm thickness. A layer of thermal oxide (5000 Å) was grown as the hard mask for silicon etching. The waveguides, parabolic reflectors, microgratings, and MEMS micromirrors were all patterned with i-line optical lithography and etched with the Applied Materials Precision 5000 etcher. A conformal layer of silicon nitride (1800 Å) was deposited by low-pressure chemical vapor deposition (LPCVD) as anti-reflection coating on the sidewall. A blank dry etching removed the silicon nitride on the top surface for the later metal deposition of the probing pads. Aluminum was deposited on the sidewall of MEMS micromirrors by e-beam evaporation with a 30° tilt angle. The backside of MEMS micromirrors was etched by a deep reactive ion etching (DRIE) using Bosch process, which consists of cycled etching and passivation steps. Plasma etching was used to remove the buried oxide for dry releasing. The chips were self-separated after the releasing step, eliminating the need for cleaving or dicing. Fig. 6 shows the SEM image of the fabricated 400-μm-pitched micromirror with rotary comb-drives. The DWDM device was fabricated similarly on a 6-inch SOI wafer. The moveable structures were released with vapor HF at 40°C. Fig. 7 shows the SEM image of the fabricated 75-μm-pitched micromirror with lateral comb-drives.

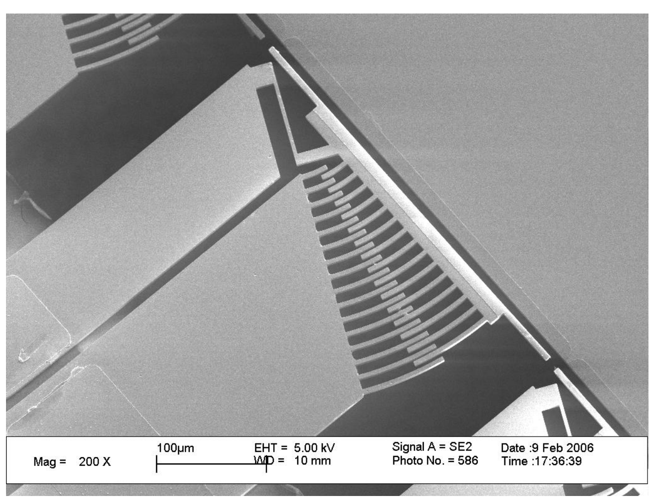

Fig. 6. SEM image of the fabricated 400-μm-pitched micromirror with rotary comb-drives.

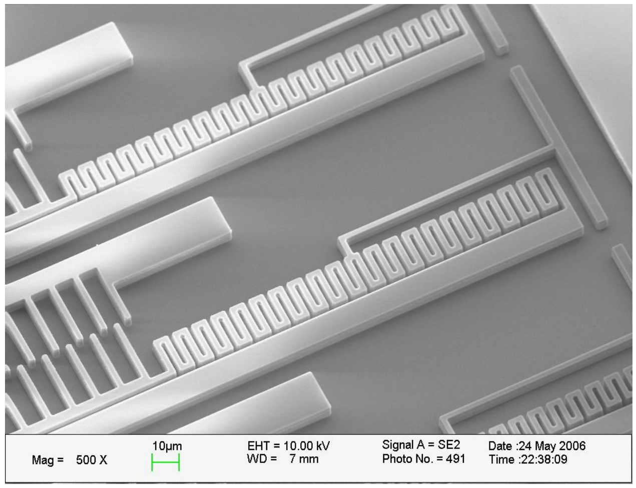

Fig. 7. SEM image of the fabricated 75-μm-pitched micromirror with lateral comb-drives.

4. EXPERIMENTAL RESULTS

4.1 MEMS micromirror characterization

The fabricated micromirrors were tested by applying a DC bias across the movable and the stationary combs. The DC characteristics of the 400-μm-pitched micromirror with rotary comb-drives are shown in Fig. 8. A maximum mechanical scan angle of 7.4° was achieved at a bias of 101 V. Fig. 9 shows the DC characteristics of the 75-μm-pitched micromirror with lateral comb-drives. A maximum mechanical scan angle of 8° was achieved at a bias of 180 V. The dependency of actuation voltage enables power equalization per port or per wavelength.

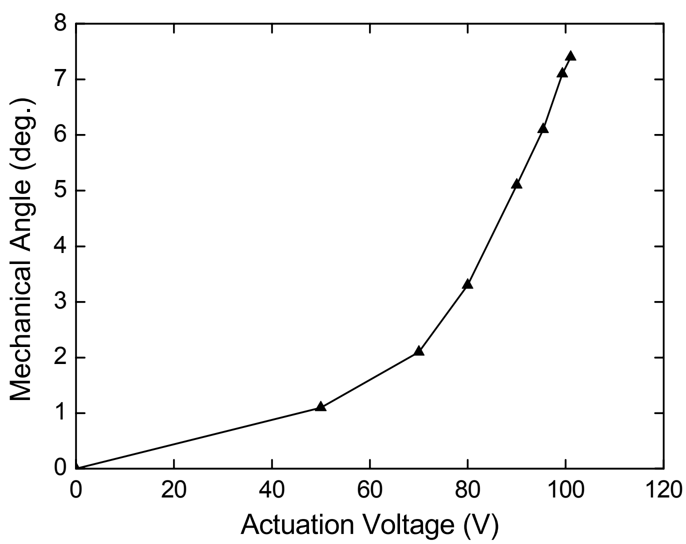

Fig. 8. DC characteristics of the 400-μm-pitched micromirror with rotary comb-drives.

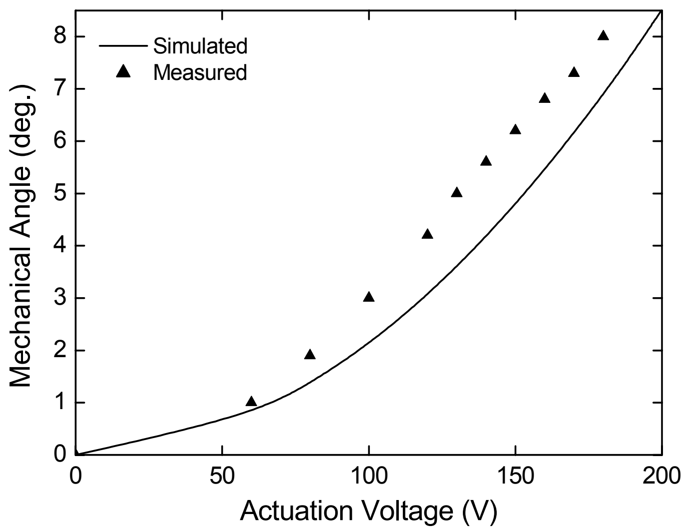

Fig. 9. DC characteristics of the 75-µm-pitched micromirror with lateral comb-drives.

4.2 Optical measurement

A lensed fiber array with 5-µm beam spot size was used to couple light to our 1x4 WSS and 4x4 WSXC. An external cavity laser tunable from 1460nm to 1580nm was used as optical source. In a 1x4 WSS, port 1 is the input and port 2 to 5 are the outputs. With micromirrors fixed at zero degree, the reflected light is coupled to port 5, which is at the symmetric position. The fiber-to-fiber insertion loss is 11.7 dB, and the crosstalk is less than -27 dB as shown in Fig. 10. In a 4x4 WSXC, signals in In 1 was split and distributed to Port 2 of WSS_1 and WSS_2, and Port 5 of WSS_3 and WSS_4. At zero bias, the signals in WSS_3 and WSS_4 were reflected to Port 1, and then sent to Out 3 and Out 4. The fiber-to-fiber insertion loss was measured to be 24 dB, which includes the 6-dB splitting loss. The crosstalk is less than -25 dB as shown in Fig. 11.

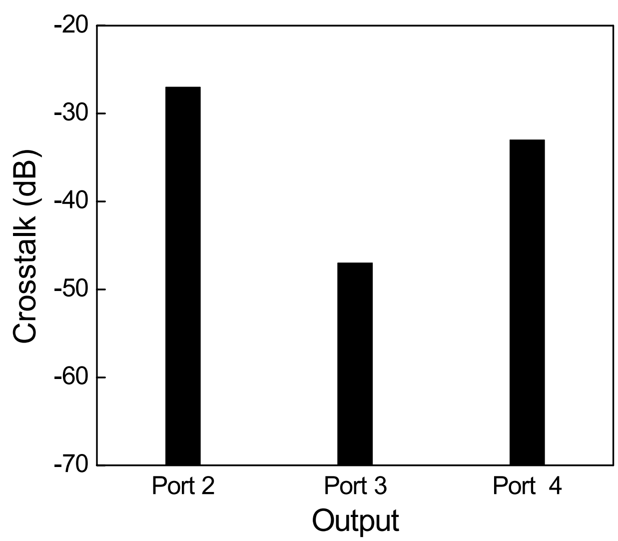

Fig. 10. Measured crosstalk on a static 1x4 wavelength-selective switch for switching from port 1 to port 5.

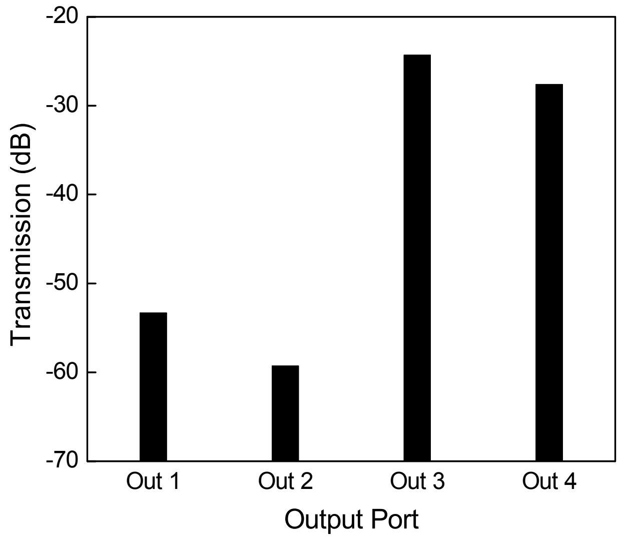

Fig. 11. Measured transmission on a static 4x4 wavelength-selective cross connect.

To gain more insight into the source of optical insertion loss, we fabricated test structures to characterize each integrated optical components. The loss is divided as follows: 2.3 dB in the round-trip fiber-waveguide coupling, 0.5 dB in the sidewall angle effect of 8 total internal reflections, 6 dB in the round-trip transmission of microgratings, 2.8 dB in diffraction loss at the 10-μm air gap, 0.4 dB in the transmission at four silicon-air interface, < 9 dB in the 1x4 MMI, 2 dB in four 90° waveguide bending, and < 1 dB in ten 90° waveguide intersections. The major discrepancy between theoretical and measured loss comes from the grating loss. Rounding and imperfect etching profile of the small triangular grating trench contributed to the extra losses. It could be improved by using reflective-type grating to reduce the loading effect.

Fig. 12 shows the temporal response for switching from port 1 to port 4 by applying a square wave. The received power is measured by a photo detector. The measured switching time (10% to 90%) is around 0.5 msec. The spectral response of wavelength-selective routing has been tested by scanning different micromirrors. Six CWDM (20-nm spacing) channels was tested with the available tuning wavelength range from 1460-1580nm.

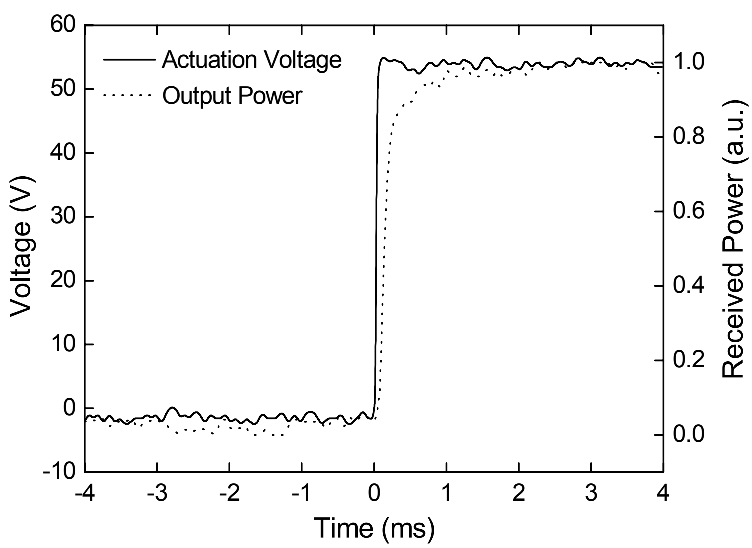

Fig. 12. Temporal response of switching from Port 1 to Port 4 on a 1x4 wavelength-selective switch.

5. CONCLUSION

We have reported on the design, fabrication, and experimental results of a monolithically integrated 1x4 WSS and 4x4 WSXC for WDM networks. The Si planar lightwave circuits and the MEMS micromirrors are monolithically fabricated on a silicon-on-insulator (SOI) wafer. The monolithic 1x4 WSS with CWDM (20-nm) channel spacing has a chip area of 1x2 cm^2, and has been experimentally characterized with a fiber-to-fiber insertion loss of 11.7 dB, and a crosstalk less than -27 dB. The monolithic 4x4 WSXC is realized by integrating four 1x4 splitters and four 4x1 WSSs. It has a chip area of 3.2x4.6 cm^2, and has been experimentally characterized with a fiber-to-fiber insertion loss of 24 dB, including a 6-dB splitting loss. The WSXC supports unicast, multicast, and broadcast functions. Wavelength-selective routing has been tested with six CWDM channels from 1460nm to 1580 nm. A 75-μm-pitched dense micromirror array has been fabricated and tested with a maximum mechanical scan angle of 8°. It enables scaling of the monolithic WSS and WSXC to DWDM (100-GHz) spacing. The solid immersion micromirror has been developed for ~3.5 times enhancement of scan angle.

This project is supported by DARPA CS-WDM program under MDA972-02-1-0020.

REFERENCE

1. K. Okamoto, M. Okuno, A. Himeno, and Y. Ohmori, "16-channel optical add/drop multiplexer consisting of arrayed-waveguide gratings and double-gate switches," Electronics Letters, vol. 32, pp. 1471-2, 1996.
2. C. R. Doerr, L. W. Stulz, D. S. Levy, R. Pafchek, M. Cappuzzo, L. Gomez, A. Wong-Foy, E. Chen, E. Laskowski, G. Bogert, and G. Richards, "Wavelength add-drop node using silica waveguide integration," Journal of Lightwave Technology, vol. 22, pp. 2755-62, 2004.
3. D. T. Fuchs, C. R. Doerr, V. A. Aksyuk, M. E. Simon, L. W. Stulz, S. Chandrasekhar, L. L. Buhl, M. Cappuzzo, L. Gomez, A. Wong-Foy, E. Laskowski, E. Chen, and R. Pafchek, "A hybrid MEMS-waveguide wavelength selective cross connect," IEEE Photonics Technology Letters, vol. 16, pp. 99-101, 2004.
4. J. E. Ford, V. A. Aksyuk, D. J. Bishop, and J. A. Walker, "Wavelength add-drop switching using tilting micromirrors," Journal of Lightwave Technology, vol. 17, pp. 904-11, 1999.
5. D. M. Marom, D. T. Neilson, D. S. Greywall, N. R. Basavanhally, P. R. Kolodner, Y. L. Low, F. Pardo, C. A. Bolle, S. Chandrasekhar, L. Buhl, C. R. Giles, S. H. Oh, C. S. Pai, K. Werder, H. T. Soh, G. R. Bogart, E. Ferry, F. P. Klemens, K. Teffeau, J. F. Miner, S. Rogers, J. E. Bower, R. C. Keller, and W. Mansfield, "Wavelength-selective 1x4 switch for 128 WDM channels at 50 GHz spacing," presented at Optical Fiber Communications Conference (OFC) 2002. Postdeadline Papers, FB7.
6. T. Ducellier, J. Bismuth, S. F. Roux, A. Gillet, C. Merchant, M. Miller, M. Mala, Y. Ma, L. Tay, J. Sibille, M. Alavanja, A. Deren, M. Cugalj, D. Ivancevic, V. Dhuler, E. Hill, A. Cowen, B. Shen, and R. Wood, "The MWS 1×4: a high performance wavelength switching building block," presented at ECOC (European Conference on Optical Communication) 2002, Session 2.3.1.
7. S. Huang, T. Jui-Che, H. Dooyoung, H. Toshiyoshi, and M. C. Wu, "Open-loop operation of MEMS WDM routers with analog micromirror array," presented at 2002 IEEE/LEOS International Conference on Optical MEMS, pp. 179-80.
8. D. M. Marom, D. T. Neilson, J. Leuthold, M. A. Gibbons, and C. R. Giles, "64 channel 4x4 wavelength-selective cross-connect for 40 Gb/s channel rates with 10 Tb/s throughput capacity," presented at ECOC (European Conference on Optical Communication) 2003, Paper We4.
9. D. M. Marom, C. R. Doerr, N. R. Basavanhally, M. Cappuzzo, L. Gomez, E. Chen, A. Wong-Foy, and E. Laskowski, "Wavelength-selective 1x2 switch utilizing a planar lightwave circuit stack and a MEMS micromirror array," presented at IEEE/LEOS Optical MEMS 2004, Paper C-1.
10. T. Ducellier, A. Hnatiw, M. Mala, S. Shaw, A. Mank, D. Touahri, D. McMullin, T. Zami, B. Lavigne, P. Peloso, and O. Leclerc, "Novel High Performance Hybrid Waveguide-MEMS 1x9 Wavelength Selective Switch in a 32-Cascade Loop Experiment," presented at ECOC 2004, Paper Th4.2.2, 2004.
11. G. Baxter, S. Frisken, D. Abakoumov, H. Zhou, I. Clarke, A. Bartos, and S. Poole, "Highly programmable Wavelength Selective Switch based on Liquid Crystal on Silicon switching elements," presented at Optical Fiber Communication Conference 2006, Paper OTuF2.
12. C. H. Chi, J. Tsai, M. C. Lee, D. Hah, and M. C. Wu, "Integrated 1x4 wavelength-selective switch with on-chip MEMS micromirrors," presented at 2005 Quantum Electronics and Laser Science Conference, Paper JThE58.

13. C. H. Chi, J. C. Tsai, D. Hah, S. Mathai, M. C. Lee, and M. C. Wu, "Silicon-Based Monolithic 4x4 Wavelength-Selective Cross Connect with On-Chip Micromirrors," presented at Optical Fiber Communications Conference (OFC) 2006, Paper OTuF1.
14. C. H. Chi, C. Hou, C. H. Lee, D. Hah, and M. C. Wu, "Silicon-Based On-Chip Micromirrors for DWDM Wavelength-Selective Crossconnects," presented at IEEE/LEOS Optical MEMS 2006, Paper P27.
15. C. H. Chi, J. Tsai, D. Hah, K. H. Jeong, and M. C. Wu, "Solid-immersion micromirror with enhanced angular deflection for silicon-based planar lightwave circuits," presented at IEEE/LEOS Optical MEMS 2005, pp. 131-2.